ESTIMATION OF HARVEST INDEX IN WHEAT CROPS USING A REMOTE SENSING-BASED APPROACH

Jaime Campoy[a*], Isidro Campos[a,1], Carmen Plaza[b], María Calera[b], Vicente Bodas[b], Alfonso Calera[a]

[a] Grupo de Teledetección y SIG. Instituto de Desarrollo Regional. Universidad de Castilla-La Mancha. Campus Universitario SN. Albacete (Spain).

[b] AgriSat Iberia S.L., Paseo de la Innovación, Nº 1, Albacete (Spain).

* Corresponding author. Email address: Jaime.Campoy@uclm.es

[1] Present address: Directorate-General of Agriculture and Rural Development. European Commission. Rue de la Loi 130. Brussels (Belgium).

Abstract

This paper presents an operational methodology for the estimation of the harvest index (HI) in commercial fields planted with wheat crops (*Triticum aestivum* L.) using a Remote Sensing based approach. The approach proposed variants from the methodologies reported by Kemanian *et al*.,(2007) and Sadras and Connor, (1991) for the estimation of the HI using the ratio between variables related with biomass production, i.e. absorbed photosynthetically active radiation (APAR), crop transpiration (T) and crop transpiration coefficient (K_t) as defined in the FAO-66 manual. The estimation of these variables along the growing season integrates time series of Remote Sensing satellite images and meteorological data into the crop growth models. The proposed models for estimation of HI were calibrated using an extensive HI dataset obtained from 19 commercial fields (empirical data) planted with wheat. The fields were subject to different water and nutrient management, resulting in empirical HI values from 0.23 to 0.55. Future applications of the proposed approach are the operational estimation of wheat production at both regional and local scales and the estimation of the within-field variability of crop production considering the variability of HI values within the field.

Keywords: *Harvest Index, NDVI, Transpiration, APAR, crop coefficient, fPAR.*

1. INTRODUCTION

Harvest index (HI) is the proportion of the total aboveground biomass that goes into harvestable parts. This concept has been developing since Beaven (1920), who established the "migration coefficient", which is defined as the proportion of dry matter of the entire aboveground plant which is accumulated in the grain. Later, Donald (1962) named this concept as Harvest Index (HI) and highlighted it as an essential parameter in terms of yield improvement. In this research line, Donald and Hamblin, (1976) proposed to estimate crop yield as the product of two factors: total aboveground biomass and HI. This approach is widely used for the estimation of crop production in crop growth models (CGMs), such as AQUACROP (Raes *et al*., 2011), EPIC (Williams *et al*., 1989) or CROPSYST (Stöckle *et al*., 2003). This paper focuses on the estimation of HI in wheat (*Triticum aestivum* L.).

According to Steduto *et al*., (2012) the differentiation of total biomass into yield using the concept of HI allows to consider the effects of stresses along the crop production process. Considering the importance of this argument, several methods have been reported for the estimation of HI. De Wit, (1958) indicated that the crop wheat biomass produced depends on the total amount water used, while HI depends on the proportion of total water used after anthesis. These findings are consistent with the ones from Passioura, (1977) and Richards and Townley-Smith, (1987). Indeed, they found a positive correlation between HI and fraction of water transpirated after anthesis. The relationship between these parameters resulted in a curvilinear fit because of the variable contribution of biomass formed before anthesis and translocated to the grain (Richards and Townley-Smith, 1987). This contribution of pre-anthesis assimilated to yield was considered by Sadras and Connor, (1991) who established a model which related positively HI and fraction of water transpirated after anthesis (ratio) and distinguished between source and sink restrictions to yield. Similarly to the latter model, Kemanian *et al*., (2007) related HI and the fraction of biomass accumulated in the post anthesis phase for several grain crops. The effect of the translocation is behind the existence of threshold

values of HI working in limited environments (i.e. water limited production) and the sink restriction results in an asymptotic relationship between the fraction of water transpirated after anthesis and HI as indicated by Sadras and Connor, (1991).

In this paper we propose a modification to the model described by Kemanian *et al*., (2007) and of the relationship obtained by Sadras and Connor, (1991) and Richards and Townley-Smith, (1987) for estimation of HI in wheat using the ratio between variables related with biomass production (i.e. crop transpiration and aboveground biomass). The innovation of the proposed approach is the estimation of the required variables using widely accepted methodologies based on Remote Sensing (RS) measurements. In this paper, we suggest to use a RS-based approach, for assessing biomass production. Our approach relies both on the well-recognized relationship among RS-based biophysical variables, crop transpiration and radiation absorption and the correlation between both variables and crop biomass production. This characteristic adds robustness to the methodology introduced and it enables its use for routine estimates at both field and regional scales.

The variables related to crop growth and biomass production in growth models are: absorbed photosynthetically active radiation (APAR), crop transpiration (T) and crop transpiration coefficient (K_t). These variables are related to biomass production through the Light Use Efficiency (LUE), Water Use Efficiency (WUE) and Water Productivity (WP*) respectively. Indeed, biomass can be estimated as the cumulated value of the product of the variables and the efficiencies. For an extensive discussion of these relationships in wheat, the reader can find further information in Campos *et al*., 2018b.

This paper aims at presenting a methodology for the estimation of HI in wheat crops using a RS-based approach and at analyzing the proposed approach using an extensive dataset of empirical data obtained in commercial fields in the Spanish region of Albacete (Southeast of Spain) under a variety of crop management and productivity. This paper also describes the potential future applications of the proposed approach such as the operational estimation of

wheat production at both regional and local scales and the estimation of the within-field variability of crop production considering the variability of HI values within the field.

2. METHODOLOGY

2.1. Equations proposed to estimate HI

The proposed approaches used for the estimation of harvest index in wheat crops are the curvilinear model described by Kemanian *et al*., (2007) see Equation 1, and the logarithmic relationship obtained by Sadras and Connor, (1991) and Richards and Townley-Smith, (1987), see Equation 2.

$$\mathrm{HI} = \mathrm{HI_x} - (\mathrm{HI_x} - \mathrm{HI_o}) \cdot \exp^{(-\mathrm{k} \cdot \mathrm{f_G})} \quad \text{Equation 1}$$

$$\mathrm{HI} = \mathrm{a} \cdot \ln(\theta_\mathrm{T}) + \mathrm{b} \quad \text{Equation 2}$$

where: HI_x and HI_o is the maximum and minimum value of HI for that crop; and f_G is the fraction of biomass accumulated in the post anthesis phase, i.e the ratio between aboveground biomass produced after anthesis over the biomass accumulation during the whole growing cycle; θ_T is the fraction of water transpired after anthesis, i.e. the ratio between accumulated transpiration during the post anthesis phase over accumulated transpiration during the entire growing cycle; k, a and b are the calibration parameters.

We present a variant of the methodologies described by these authors as presented in the Equation 3 and Equation 4. The main difference is that the variables used as a proxy of wheat biomass production in the model proposed by Kemanian *et al*.,(2007) were the accumulated values of absorbed photosynthetically active radiation (APAR), crop transpiration (T) and the product of the crop transpiration coefficient (K_t) and the cold stress coefficient (K_{st}). The main difference with the model proposed by Sadras and Connor, (1991) is that the ratio θ_T was based on a remote sensing based approach and we also evaluated that the estimation of HI is based on the fraction of the driving variables APAR and $K_t \cdot K_{st}$ accumulated after anthesis. In this

manner, both models were analyzed in this work using the 3 possible approaches (APAR, T and $K_t \cdot K_{st}$) for the estimation of θ.

$$HI = HI_x - (HI_x - HI_o) \cdot \exp^{(-k \cdot \theta)} \quad \text{Equation 3}$$

$$HI = a \cdot \ln(\theta) + b \quad \text{Equation 4}$$

where: θ is the ratio between the variable related with the biomass production accumulated after anthesis over the same variable accumulated during the whole growing cycle and the sub-indexes $_{APAR}$, $_{T}$ or $_{Kt \cdot Kst}$ refers to the three approaches analyzed in this work.

The relationship between biomass production and the proposed variables (APAR, T and $K_t \cdot K_{st}$) derives from RS methodologies has been demonstrated in previous experiences for wheat (Campos *et al*., 2018a,b). The present study outreaches the existing framework and suggests to apply such relationships to assess HI. The main objective in commercial farms is a robust estimation of yield. However, the mechanistic analysis of the crop productivity at a scientific level requires the investigation of the various components of the yield and this paper focuses on the estimation of HI. The conclusions obtained can be used in further investigations or operational applications.

2.2. Estimation of APAR, T and K_t using remote sensing data

Interception of PAR (IPAR) and absorption of PAR (APAR) have a similar numerical value, considering a low proportion of non-photosynthetic elements in the canopy (Asrar *et al*., 1984). APAR can be estimated as the product of the incident PAR (PAR_{in}, $MJ \cdot m^{-2}$) and the fraction of PAR_{in} intercepted by the vegetation (fPAR, dimensionless), (Equation 5). According to Szeicz, (1974) PAR_{in} is about 50% of the incident solar radiation.

Transpiration (T) is calculated as the product of the transpiration coefficient (K_t, dimensionless) times reference evapotranspiration (ETo, $mm \cdot day^{-1}$), (Steduto *et al*., 2012), see Equation 6. K_t defined by Steduto *et al*., (2012) is similar to the basal coefficient (K_{cb}) proposed by Allen *et al*., (1998) to estimate transpiration, However, the difference between K_t and K_{cb} is

more evident in the absolute value under bare soil conditions. K_t is equal to 0 under bare soil conditions and it reaches its maximum value, similar to K_{cb}, when the crop reaches the full cover. For further information, Campos *et al*., (2017) provide a well-documented analysis of the convenience to use K_t for estimating crop biomass.

$$\mathrm{APAR} = \mathrm{fPAR} \cdot \mathrm{PAR_{in}} \quad \text{Equation 5}$$

$$\mathrm{T} = \mathrm{K_t} \cdot \mathrm{ETo} \quad \text{Equation 6}$$

The main challenge of the proposed formulations is to estimate the temporal evolution of biophysical parameters fPAR and K_t. Time series of remote sensing offer a unique opportunity to describe and monitor spatial and temporal evolution of the canopy and these variables. Thus, the methodology proposed to estimate K_t and fPAR is based on their relationships with the Normalized Differential Vegetation Index (NDVI). In this work, NDVI data were obtained from time series of multispectral imagery at high temporal and spatial resolution from Landsat8 (L8) and Sentinel 2 (S2A, S2B).

In this work, fPAR was estimated using the relationship defined by Sellers *et al*., (1996), see Equation 7. These authors propose a methodology to estimate fPAR based on rescaling NDVI values between the minimum NDVI and fPAR values in the area (bare soil conditions) and the maximum NDVI and fPAR values (maximum values reached by the crop), see Equation 8. This equation is similar to the formulations published by Asrar *et al*., (1984) for wheat (1.25·NDVI-0.11) and Daughtry *et al*., (1992) for maize and soybean (1.25·NDVI-0.21).

$$\mathrm{fPAR} = \frac{(\mathrm{NDVI} - \mathrm{NDVI_{min}}) \cdot (\mathrm{fPAR_{max}} - \mathrm{fPAR_{min}})}{(\mathrm{NDVI_{max}} - \mathrm{NDVI_{min}})} + \mathrm{fPAR_{min}} \quad \text{Equation 7}$$

where $fPAR_{max}$ = 0.95 and $fPAR_{min}$ = 0.001 proposed by Sellers et al., (1996); NDVImin (0.15−0.18) and NDVImax (0.91−0.93) in the area.

$$\mathrm{fPAR} = 1.26 \pm 0.03 \cdot \mathrm{NDVI} - 0.21 \pm 0.02 \quad \text{Equation 8}$$

The relationship selected to estimate K_t is based on the re-scaling NDVI values methodology proposed by Choudhury *et al*., (1994) and modified by González-Dugo and Mateos, (2008), see Equation 9. This methodology rescales NDVI values between the minimum NDVI

value in the study area (bare soil) and the maximum NDVI value corresponding to the maximum K_t reached by the crop (see Equation 10). This equation is similar to the relationship proposed by Duchemin et al., (2006) for wheat (1.64·(NDVI-0.14)).

$$K_t = K_{t,max} \cdot \left[1 - \left(\frac{(NDVI_{max} - NDVI)}{(NDVI_{max} - NDVI_{min})}\right)^{\alpha}\right] \quad \text{Equation 9}$$

where $K_{t,max}$ =1.15 proposed in FAO-56 manual (Allen *et al.*, 1998); NDVImin (0.15−0.18) and NDVImax (0.91−0.93) in the area; and α = 1, linear relationship (Calera *et al.*, 2017).

Based on the previous parameters, it is possible to approach this relationship with Equation 10.

$$K_t = 1.52 \pm 0.04 \cdot NDVI - 0.25 \pm 0.02 \quad \text{Equation 10}$$

2.3. Estimation of water and cold stresses

Water deficit is the most common stress in the study area. According to Steduto *et al.*, (2012) water stress and reduced transpiration result on a reducing rate of biomass production that can decline the crop yield. Water stress induces different effects on the development of canopy. Initially, water stress causes a reduction of expansion and growth of the canopy due to reduced turgor pressure in plants that induces a decrease in processes such as leaf expansion and tillering (Ritchie, 1998). Canopy's growth reduction of can be reflected by time series NDVI images derived from satellites. However, if water deficit continues, actual transpiration will be reduced mainly by partially closed stomata (Hsiao, 1973) and potential biomass rate to be reduced in the same proportion as the transpiration (Ritchie, 1998). Thus, the effect of water stress on reducing rate of biomass production, and hence APAR, T and K_t, should be included in the models based on APAR, T and K_t through the water stress coefficient (K_{sw}), see Equation 11, Equation 12 and Equation 13.

$$\int_{t_0}^{t} APAR_{adj}\, d(t) = \int_{t_0}^{t} fPAR \cdot K_{sw} \cdot PAR_{in}\, d(t) \quad \text{Equation 11}$$

$$\int_{t_0}^{t} T_{adj}\, d(t) = \int_{t_0}^{t} K_t \cdot K_{sw} \cdot ETo\, d(t) \quad \text{Equation 12}$$

$$\int_{t_0}^{t} K_{st} \cdot \frac{T_{adj}}{ETo}\, d(t) = \int_{t_0}^{t} K_{st} \cdot K_{t,adj}\, d(t) = \int_{t_0}^{t} K_{st} \cdot K_t \cdot K_{sw}\, d(t) \qquad \text{Equation 13}$$

Where $APAR_{adj}$ is the PAR absorbed under water stress conditions in $MJ \cdot m^{-2}$; T_{adj} is the crop transpiration under water stress conditions in mm; $K_{t,adj}$ is the crop transpiration coefficient accounting for water stress conditions, dimensionless; K_{sw} is the crop water stress coefficient, dimensionless; K_{st} is the cold temperature stress coefficient for biomass production, dimensionless; variables are accumulated during the period between t_0 and t.

In this work, K_{sw} is estimated by an approach based on a soil water balance model compiled in the FAO 56 manual (Allen *et al.*, 1998). This methodology requires a daily water balance for the root zone. According to the FAO 56 manual, when soil water is abstracted by evapotranspiration, water depletion in the root zone (Dr) increases and stress will appear when depletion becomes equal to readily available water (RAW). If depletion continue to increase, K_{sw} decreases linearly. RAW is expressed as product of TAW (total available soil water in the root zone,) times p (fraction of TAW that a crop can extract from the root zone without suffering water stress), see Equation 14. K_{sw} values vary from 1 when the effect of water stress is nonexistent, to 0 when this effect is maximum. The estimation of Dr is described in the FAO-56 manual (Allen *et al.*, 1998) and the value of p used in this study was 0.55, as proposed in this manual.

$$K_{sw} = \frac{TAW - Dr}{TAW - RAW} = \frac{TAW - Dr}{(1 - p) \cdot TAW} \qquad \text{Equation 14}$$

This approach integrates basal crop coefficient (K_{cb}) derived from time series NDVI of satellite images into the daily soil water balance model widely explained in the FAO 56 manual. This methodology is well-documented in literature: Campos *et al.*, (2017), Gonzalez-Dugo *et al.*, (2009), Padilla *et al.*, (2011), Campos *et al.*, (2016)).

K_{sw} was considered in the model only for those fields where crop suffered water deficit during the growing season. Thus, water stress K_{sw} was only considered in the model in all rain-

fed fields and two irrigation fields (2 and 7). K_{sw} was estimated using meteorological data registered in the area and actual irrigation data provided by farmers. No information on soil properties is available in study plots. Root development is frequently limited in the area because of the presence of limestone bedrocks from 0.5 to 1 m. Simulations of soil water balance was realized considering a typical soil in the study area, i.e. a TAW of 100 mm, equivalent to a maximum root depth of 60 cm. Root depth and consequently TAW was interpolated between the maximum and minimum values based on the K_{cb} values as proposed in the FAO-56 manual. The assumption of a standard soil for every field is based on our experience in the area, we consider that this is a reasonable hypothesis and allows the evaluation of the model without the uncertainty caused by the variability of the soil conditions not fully justified with empirical evidences. The implementation of this approach in other areas will requires specific knowledge and the useful guidelines are in the FAO-56 manual (Allen et al. 1998).

The formulation of Equation 13 includes the cold stress coefficient for biomass production (K_{st}) to modulate biomass production under cold weather conditions, and to modulate the accumulation of K_t. The effect of temperature on reducing the accumulation of crop biomass is reported in the literature (Brown *et al*., (2006), Campos *et al*., (2017), Campoy *et al*., (2019)). In this work , estimation of K_{st} is based in the methodology proposed by Raes *et al*., (2011), following a logistic function and the knowledge of thresholds of growing degree days (GDD) for the production of biomass. According to FAO-66 manual (Steduto *et al*., 2012), the optimum growth in wheat crops occurs at 14ºC and the lower limit for biomass production is 0ºC.

In the proposed formulation, the effect of the stresses on HI is reflected through the variation of θ. In addition, this paper analyzes the impact of water stress on the variability of θ for the most stressed fields during two growing seasons. It discusses the possible application of the proposed approaches considering exclusively the variables derived from the temporal evolution of NDVI and meteorological variables. The cold stress coefficient was not included in

the models based on T and APAR. It could be a double correction of this stress because ETo and PAR_{in} are related with the temperature. The effect of fertilization stress (nitrogen) is discussed in the discussion section and the salinity stress cannot be tested with the available dataset. It was excluded from the formulation but all stresses might affect the biomass production and should be included in future applications.

2.4. Definition of growing season

In this work, the length of the growing cycles were delimited using NDVI thresholds. Thus, the growing cycles were defined individually for each pixel in order to estimate accumulated variables. Time series of NDVI allow to identify of the beginning of the growing season. This period named green-up is identified as the inflection of the NDVI curve coinciding with the beginning of the tillering stage. Threshold of NDVI in green-up reaches a value of 0.3, according to Lobell *et al*., (2013) and González-Gómez *et al*., (2018) and this threshold value was used in this work. The end of the growing season was established as the physiological maturity stage (BBCH 85-87) as wheat crops reach the maximum accumulated biomass. The exact dates of these stages were determined in the ground for the collection of the biomass and yield data as presented below. The main weakness for estimating the ratio (θ) is the knowledge of the exact date of full flowering (BBCH-65). In this work, the date of flowering was extrapolated from the direct observation and the phenological monitoring of each field, see Table 2.

Figure 1 shows the crop growing cycle for the Field 1 defined by the time series of NDVI images and the key featured dates green up, maturity grain and flowering) used to delimit the accumulation of the studied variables (APAR, T and $K_t \cdot K_{st}$). The accumulated variables are computed during the entire crop growing and during the reproductive phase for the estimation of θ. In absence of water stress, the integral or the area under the curve described by the temporal evolution of K_t versus the accumulated reference evapotranspiration (ETo) represents the accumulated crop transpiration (T), according Equation 12, see Figure 2. In this way, the

proportion between the reproductive phase and the complete growing cycle is easy to visualize. In the example from Figure 2, the crop accumulated half of total T during the reproductive phase and the value of θ_T was around 0.5.

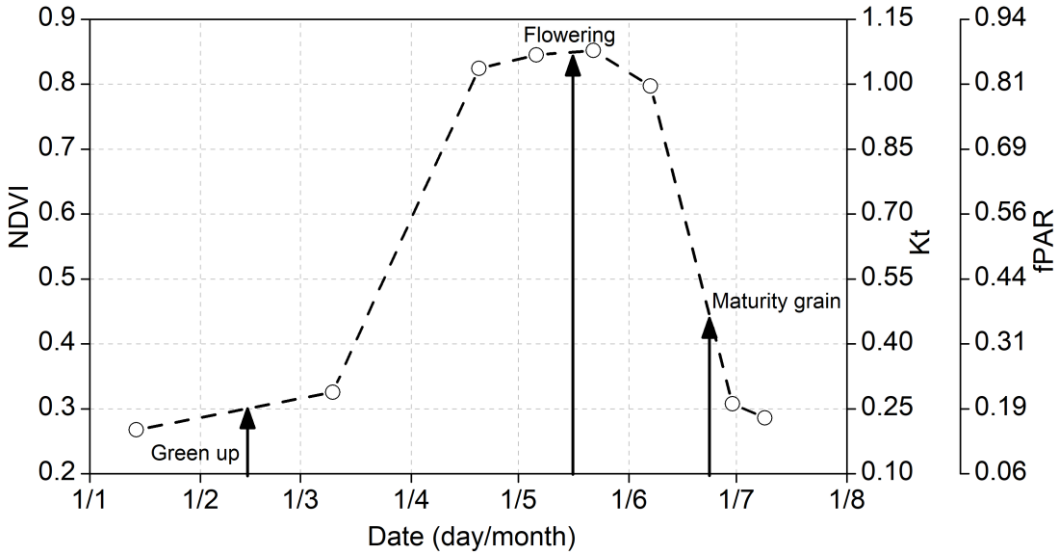

Figure 1. Temporal evolution of the measured NDVI (white circles), interpolated values of NDVI, daily values of the transpiration coefficient (K_t) and fraction of PAR_{in} intercepted by the vegetation (fPAR) (dash line) for the Field 1.

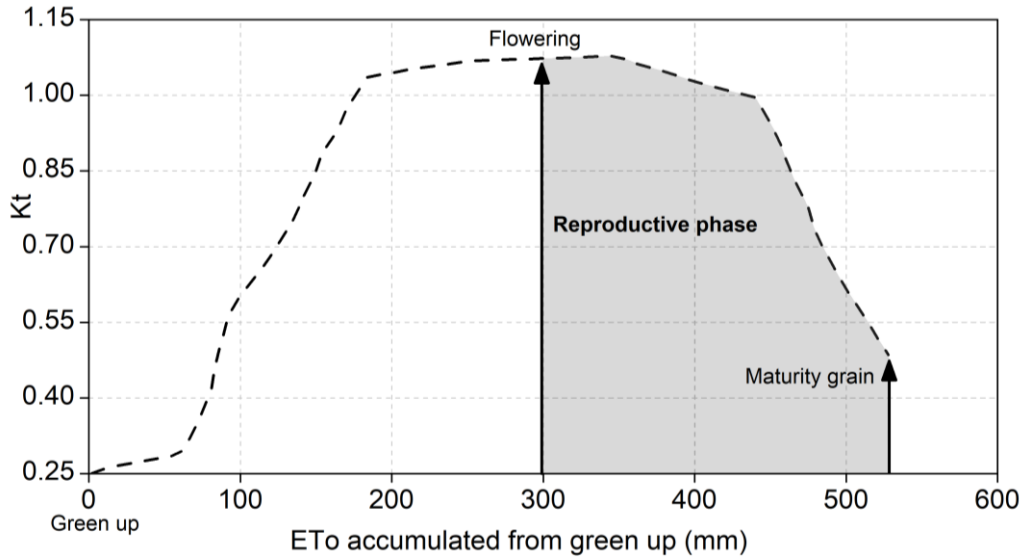

Figure 2. Temporal evolution of transpiration coefficient (K_t) (dash line) versus the accumulated reference evapotranspiration (ETo) (mm), which is used as thermal time, from green up to maturity for the Field 1. The area under the curve is the accumulated crop transpiration (T).

2.5. Calibration of the HI equations

The calibration parameters proposed by Kemanian *et al.*, (2007) for wheat provided a plausible estimation of the actual values of HI empirically measured in this work. However, the use of the calibration parameter k and the limits of HI proposed by these authors (HI_x and HI_o) implies that the minimum HI obtained in any conditions will be around 0.3. On the other hand, the use of the calibration parameter b proposed by Sadras and Connor, (1991) and Richards and Townley-Smith, (1987) determines that the maximum value of HI will be 0.47-0.50. In the authors' view, these assumptions should be demonstrated empirically and the procedure described in this section allowes the calibration of the Equation 3 and Equation 4 using empirical data.

The exponential and logarithmic functions, proposed in Equation 3 and Equation 4 respectively, are linearized to estimate the calibration parameters (k, a and b). Linearizing equations is a process of modifying an equation to produce new variables which can be plotted to produce a straight line graph. Later, using empirical HI data and the estimates of θ using the 3 possible approaches (APAR, T and $K_t \cdot K_{st}$), we obtained the empirical relationships between HI and θ proposed in this study. The Table 1 summarizes the variables used in the model and the calculation procedures used in this analysis.

Table 1. Summary of the management in fields analyzed in this work.

Symbol	Description	Procedure
θ	Ratio between the variable related with the biomass production: APAR, T or $K_t \cdot K_{st}$	Estimated
k, a and b	Calibration parameters	Calibrated using empirical data of HI
APAR	Absorbed photosynthetically active radiation	Estimated
PAR_{in}	Incident PAR	Measured
fPAR	Fraction of PAR_{in} intercepted by the vegetation	Estimated based on NDVI relationship
T	Transpiration	Estimated
ETo	Reference evapotranspiration	Measured
K_t	Transpiration coefficient	Estimated based on NDVI relationship
K_{sw}	Water stress coefficient	Estimated
K_{st}	Cold temperature stress coefficient for biomass production	Estimated
Dr	Water depletion in the root zone	Estimated
TAW	Total available soil water in the root zone	Estimated
RAW	Readily available water	Estimated
p	Fraction of TAW that a crop can extract without suffering water stress	Estimated

3. GROUND MEASUREMENTS AND SATELLITE DATA

3.1. Study sites and fields monitored

Field data was obtained in commercial fields located in the province of Albacete (South-East of Spain). The climate in the study area is Mediterranean; the mean annual temperature and precipitation over the past 30 years were 13.6ºC and 340 mm, respectively.

Study fields were selected to cover an extensive range of average yields (1.2 – 10.3 t/ha). This range of yield also resulted in a wide range of HI values, which is a valuable dataset to analyze and parameterize HI values in commercial fields. The range of yield reported in this study represents the maximum and minimum wheat production in the area and are obtained under irrigated and rain-fed conditions respectively. The dataset was obtained in 19 commercial fields (Fields 1-19) monitored in four campaigns (2015, 2016, 2017 and 2018). The monitored fields were managed with different water conditions (rain-fed and irrigated fields) and nutrient managements, and following traditional tillage and direct seeding (see Table 2).

Growing cycles and management differ for irrigated and rain-fed varieties cultivated in the area. The growing cycle in irrigated varieties (spring wheat) spans from January to July and in rain-fed varieties (winter wheat) spans from November to June. All irrigated fields monitored in this study used center pivot systems and were irrigated following the water crop requirements, except for fields 2 and 7 where the crop suffered water stress conditions. Water shortage was evidenced by the soil water balance model implemented and it is also reflected in the lower production registered.

Fertilization was applied following local practices. In rain-fed fields, the fertilizer was applied before seeding and during the phase of tillering. In irrigated fields, fertilizer was applied in different portions during crop development. Table 2 shows the geographical coordinates, area, cultivated varieties, management practices, total amounts of irrigation and fertilization applied, yield, harvest index, number of sampling zones and date of full flowering obtained in each field.

Table 2. Summary of the management in fields analyzed in this work.

Field ID	Year monitored	Coordinates	Surface (ha)	Variety	Management	Irrigation (rainfall) (mm)	Fertilization kg/ha (N,P,K)	Yield (kg/ha)	HI	Sampling zones	Date full flowering
1	2015	39.2523 N, 1.9986 W	30.7	Califa	Irrigated, direct seeding	452 (147)	257,81,65	8836	0.52	9	12/05/2015
2	2015	39.0790 N, 1.6568 W	35.9	Galera	Irrigated, direct seeding	230 (93)	140,79,0	3819	0.41	9	23/05/2015
3	2015	38.8748 N, 1.8374 W	41.6	Califa	Irrigated, conventional	447 (117)	268,120,150	7421	0.50	9	15/05/2015
4	2016	39.2526 N, 1.9903 W	41.0	Califa	Irrigated, direct seeding	453 (148)	218,105,34	7449	0.43	6	23/05/2016
5	2016	38.8912 N, 1.8711 W	46.6	Califa	Irrigated, conventional	461 (118)	349,132,165	10261	0.47	6	25/05/2016
6	2016	39.1324 N, 1.9097 W	26.6	Califa	Irrigated, conventional	480 (171)	294,129,55	9402	0.43	6	16/05/2016
7	2016	39.0627 N, 1.6752 W	31.9	Galera	Irrigated, direct seeding	240 (123)	113,0,0	4758	0.38	6	23/05/2016
8	2017	39.2576 N, 1.9956 W	38.5	Califa	Irrigated, direct seeding	440 (101)	257,104,124	8533	0.45	3	16/05/2017
9	2017	38.8453 N, 1.9099 W	34.8	Califa	Irrigated, conventional	568(116)	278,126,158	8652	0.46	3	16/05/2017
10	2017	39.2549 N, 1.3886 W	11.1	PR22	Rainfed, direct seeding	(82)	68,46,0	1634	0.39	3	01/05/2017
11	2017	39.2552 N, 1.3939 W	3.8	PR22	Rainfed, direct seeding	(82)	68,46,0	1180	0.38	3	01/05/2017
12	2017	39.2627 N, 1.9891 W	7.7	Sarina	Rainfed, direct seeding	(159)	88,57,0	2277	0.34	3	01/05/2017
13	2017	39.2699 N, 1.9914 W	12.1	Sarina, PR22	Rainfed, direct seeding	(137)	88,57,0	2134	0.32	3	01/05/2017
14	2017	38.8220 N, 1.8603 W	48.5	Sarina	Rainfed, direct seeding	(110)	58,0,60	1921	0.34	3	01/05/2017
15	2018	39.2743 N, 1.9695 W	18.3	Sarina	Rainfed, direct seeding	(265)	97,66,0	1987	0.33	3	16/05/2018
16	2018	39.2748 N, 1.9849 W	7.4	Sarina	Rainfed, direct seeding	(283)	97,66,0	2354	0.38	3	16/05/2018
17	2018	39.2703 N, 1.2309 W	14.3	Sarina	Rainfed, direct seeding	(172)	50,0,0	2116	0.41	3	16/05/2018
18	2018	39.2330 N, 1.2766 W	20.3	Sarina	Rainfed, direct seeding	(225)	50,0,0	2633	0.37	3	16/05/2018
19	2018	38.8348 N, 1.8506 W	86.2	Sarina	Rainfed, direct seeding	(201)	46,0,0	1949	0.45	12	16/05/2018

3.2. HI Field data

The main ground measurements used in this study was harvest index (HI) data measured in the study fields. HI was obtained as the relationship of dry biomass yield components (grain) over total dry aboveground biomass. HI was measured at time of physiological maturity stage, when crop reaches maximum aboveground biomass. As indicated in the literature, *Dodds et al*., (1979), Calderini *et al*., (2000), wheat crop reached approximately 35% of kernel water concentration in this stage. According with our experience, this stage corresponded to the phenological stages 85-87 in the BBCH scale. Therefore, two parameters were used to determine the time of biomass collection: humidity grain estimated in the field using a grain humidity sensor (Wile 55 grain moisture meter, Farmcomp, Tuusula, Finland) and the visual determination of the phenological stage.

Dry biomass measurement included the whole plant (leaves, stems, heads and grains) excluding roots. The samples of aboveground biomass were obtained at 3-12 measurement locations (sampling zones) in each field. Each sample was composed of 3 sub-samples separated about 10 m. In each sub-sample, aboveground biomass was collected manually along a 1.5 m length in two adjacent rows. Later, biomass was dried in an oven at 60ºC until the weight was stabilized and measured. The data obtained in each sub-sample is presented in the Annex I.

Sampling zones were situated in a homogeneous area, with approximately 1 ha. These areas were delimited using maps of potential biomass production of precedent crops using time series of satellite images (Campos *et al*., 2018a). In this manner, different zones were defined in each field with low, medium and high potential productivity for the location of the sampling zones, see Table 2.

3.3. Remote Sensing and meteorological data

In this paper, time series used NDVI images derived from a virtual constellation formed by Landsat 8 (L8) and Sentinel 2 (S2A, S2B) satellites. The high temporal frequency obtained

(around 1 image for week) allowed to describe the crop growing cycle and estimate accurately the biophysical parameters used in the study. Temporal evolution of NDVI was interpolated linearly on a daily scale using the adjacent satellite images. Atmospheric effects and possible differences between calibrations of the used sensors were compensated using a procedure of absolute normalization of the NDVI. This method is based on the selection of pseudo-invariant surfaces (dense vegetation and agricultural bare soil), (Chen *et al*., 2005).The acquisition dates of the images used in the study for each field are shown in Table 3. The temporal evolutions of K_t and fPAR derived from time series NDVI images were estimated in an area of 3 by 3 pixels centered in the sampling zones. Spatial resolution depends on the satellite images used, 30 m for Landsat 8 and 10 m for Sentinel 2, being sufficient resolution to monitor the homogeneous areas (around 1 ha).

Meteorological data necessary in this work were obtained from the National Meteorological Services SIAR (Servicio Integral de Asesoramiento al Regante, http://crea.uclm.es/siar/) and the closest station were selected for the analyses performed in each field, see Table 3. Meteorological data used in this study included the daily reference evapotranspiration (ETo) calculated using the FAO-56 Penman-Monteith equation for grass (Allen *et al.*, 1998), maximum and minimum daily temperature, average daily incoming solar radiation and cumulative daily precipitation.

Table 3. Dates of the images and Station SIAR used in the analysis.

Field ID	**Dates of Images (dd/mm/yy)**	**Station SIAR**
1	**L8**: 14/01/15, 10/03/15, 20/04/15, 06/05/15, 22/05/15, 07/06/15 , 30/06/15, 09/07/15	La Gineta
2	**L8**: 14/01/15, 10/03/15, 20/04/15, 06/05/15, 22/05/15, 07/06/15 , 30/06/15	Albacete
3	**L8**: 10/03/15, 06/05/15, 22/05/15, 07/06/15, 30/06/15, 09/07/15	Albacete
	L8: 09/06/16, 02/07/16	
4	**S2A**: 04/02/16, 12/03/16, 25/03/16, 01/04/16, 24/04/16, 01/05/16, 21/05/16, 13/06/16, 20/06/16, 23/06/16	La Gineta
	L8: 31/05/16, 02/07/16	
5	**S2A**: 04/02/16, 12/03/16, 25/03/16, 01/04/16, 14/04/16, 24/04/16, 01/05/16, 21/05/16, 13/06/16, 20/06/16, 23/06/16	Albacete
	L8: 17/01/16, 24/01/16, 02/07/16	
6	**S2A**: 03/12/15, 04/02/16, 12/03/16, 25/03/16, 24/04/16, 01/05/16, 21/05/16, 10/06/16, 13/06/16, 20/06/16, 23/06/16	La Gineta

7	**L8**: 24/01/16, 31/05/16, 09/06/16 **S2A**: 04/02/16, 12/03/16, 25/03/16, 24/04/16, 01/05/16, 21/05/16, 13/06/16, 20/06/16	Albacete
8	**L8**: 12/06/17 **S2A**: 08/02/17, 25/02/17, 10/03/17, 20/03/17, 06/04/17, 09/04/17, 06/05/17, 09/05/17, 19/05/17, 05/06/17, 18/06/17 **S2B**: 30/06/17	La Gineta
9	**L8**: 12/06/17 **S2A**: 08/02/17, 25/02/17, 10/03/17, 20/03/17, 06/04/17, 09/04/17, 06/05/17, 19/05/17, 05/06/17, 15/06/17, 18/06/17 **S2B**: 30/06/17	Albacete
10	**L8**: 27/05/17, 12/06/17 **S2A**: 18/02/17, 25/02/17, 10/03/17, 20/03/17, 30/03/17, 06/04/17, 06/05/17, 09/05/17, 19/05/17	Campo Arcís (Requena)
11	**L8**: 27/05/17, 12/06/17 **S2A**: 18/02/17, 25/02/17, 10/03/17, 20/03/17, 30/03/17, 06/04/17, 06/05/17, 09/05/17, 19/05/17	Campo Arcís (Requena)
12	**L8**: 03/01/16, 27/05/17 **S2A**: 17/11/16, 08/02/17, 25/02/17, 10/03/17, 20/03/17, 09/04/17, 06/05/17, 09/05/17	La Gineta
13	**L8**: 03/01/16, 27/05/17 **S2A**: 17/11/16, 08/02/17, 25/02/17, 10/03/17, 20/03/17, 09/04/17, 06/05/17, 09/05/17	La Gineta
14	**L8**: 02/05/16, 27/05/17 **S2A**: 16/01/17, 25/02/17, 10/03/17, 20/03/17, 09/04/17, 09/05/17, 19/05/17, 05/06/17	Pozocañada
15	**S2A**: 01/01/18, 21/01/18, 22/03/18, 14/04/18, 04/05/18, 13/06/18, 20/06/18 **S2B**: 16/01/18, 08/02/18, 25/02/18, 07/03/18, 26/04/18, 09/05/18, 16/05/18	La Gineta
16	**S2A**: 01/01/18, 21/01/18, 22/03/18, 14/04/18, 04/05/18, 13/06/18, 20/06/18 **S2B**: 16/01/18, 08/02/18, 25/02/18, 07/03/18, 26/04/18, 09/05/18, 16/05/18	La Gineta
17	**L8**: 28/04/18 **S2A**: 21/01/18, 22/03/18, 31/05/18, 20/06/18 **S2B**: 25/02/18, 07/03/18, 27/03/18, 16/05/18, 15/06/18	Campo Arcís (Requena)
18	**L8**: 07/02/18, 28/04/18 **S2A**: 21/01/18, 24/01/18, 22/03/18, 14/05/18, 31/05/18, 13/06/18, 20/06/18 **S2B**: 25/02/18, 07/03/18, 19/04/18, 15/06/18	Campo Arcís (Requena)
19	**S2A**: 22/03/18, 14/04/18, 04/05/18, 21/05/18, 13/06/18, 20/06/18, 23/06/18 **S2B**: 25/02/18, 16/05/18,	Pozocañada

4. RESULTS

4.1. Assessment of the crop growing cycles.

The NDVI images time series were used to define the crop growing cycle at field and at pixel scales. Table 4 summarizes the lengths of the crop growing cycles and climatic data collected from green-up to maturity in the study fields determined using the methodology proposed.

All analyzed fields present similar climatological conditions due to their geographic proximity, see Table 4 and Figure 3a. However, differences in the planting dates, length of the

growing cycle and specific meteorological conditions resulted in variations in the mean temperature, solar radiation and accumulated ETo. Accumulated ETo during the whole growing cycle in the irrigated fields was, on average, 40% higher than ETo accumulated for the rain-fed fields. These differences in the lengths of the crop growing cycles are shown in the Figure 3b, which describes canopy growth by the temporal evolution of NDVI in the fields 1, 13 and 16.

The water balance indicates that only the rain-fed and water deficit fields suffered from evident water stress conditions and the reason was the irrigation management practices (i.e. irrigation timing and total amount). Temporal evolution of K_{sw}, see Figure 3c, shows a first phase (November-April) which crops growths with no water stress conditions, and accumulated biomass with no limitations. However, in a second phase (April-June), severe water stress conditions induce on reducing rate of transpiration (K_{sw}<1). Most of the second phase coincides on time with reproductive phase, which begins with the full flowering phenological stage (BBCH-65) during the first half of May.

Table 4. Lengths of the crop growing cycles and meteorological data collected from green-up to maturity in the study fields.

Field	Year monitored	Crop Growing Cycle (days)	Accumulated ETo (mm)	Mean ETo (mm)	Mean Tª (ºC)	Mean PAR_{in} ($MJ \cdot m^{-2}$)
1	2015	127	528	4.1	13.6	10.0
2	2015	93	406	4.2	14.6	10.6
3	2015	102	452	4.4	15.2	10.8
4	2016	126	503	4.0	12.6	10.0
5	2016	132	538	4.0	12.9	9.9
6	2016	171	567	3.3	11.2	8.4
7	2016	127	444	3.5	11.2	8.8
8	2017	116	499	4.3	14.4	10.6
9	2017	114	510	4.4	14.5	11.2
10	2017	89	325	3.6	12.8	9.8
11	2017	85	313	3.6	12.9	9.8
12	2017	153	380	2.5	8.5	7.1
13	2017	148	376	2.5	8.6	7.3
14	2017	115	358	3.1	11.8	8.8
15	2018	126	394	3.1	9.6	8.4
16	2018	129	393	3.0	9.4	8.2
17	2018	100	375	3.7	13.5	9.5
18	2018	118	406	3.4	12.5	8.9
19	2018	93	323	3.4	11.6	9.4

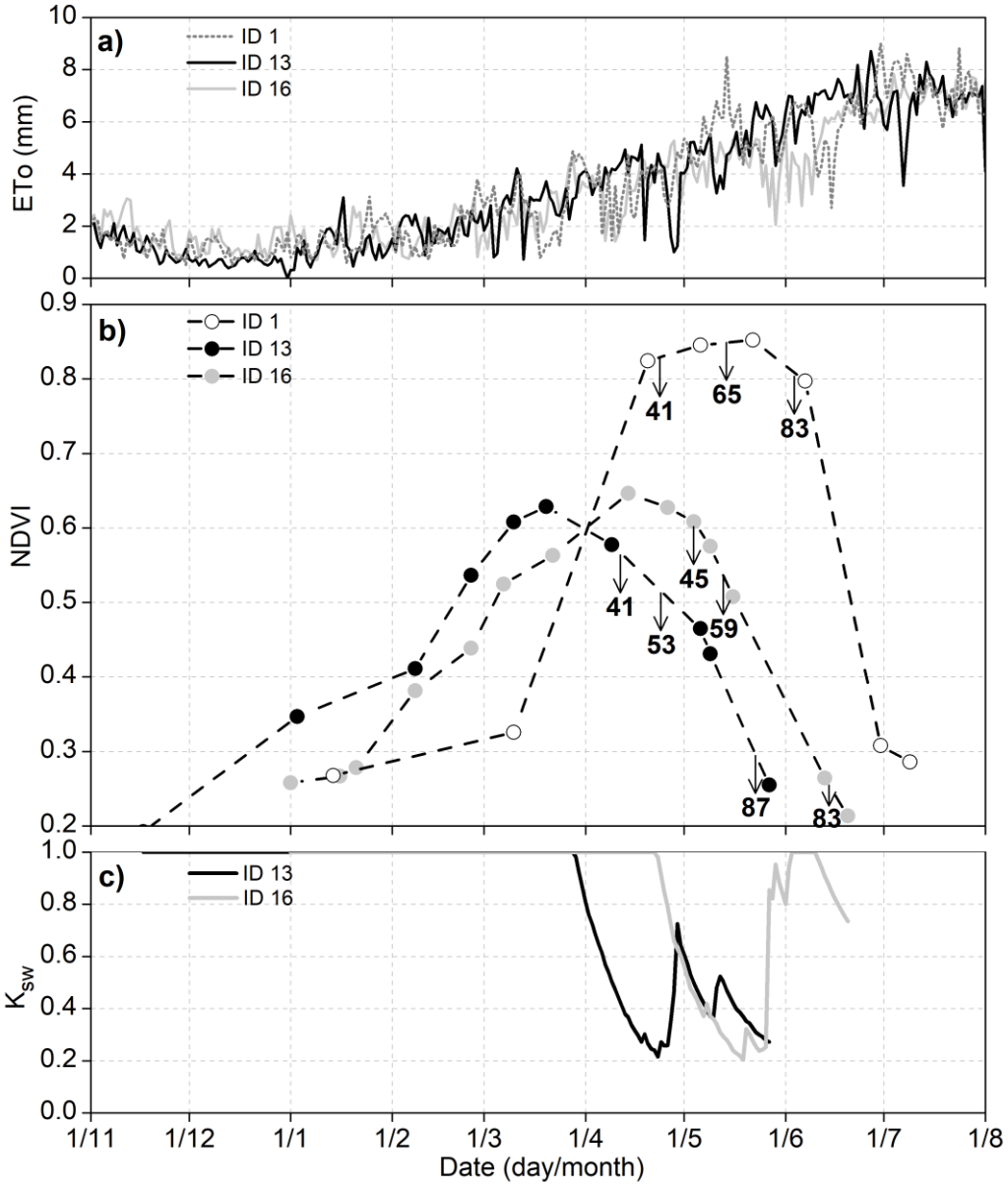

Figure 3. a) Temporal evolution of the reference evapotranspiration (ETo) for fields 1 (irrigated), 13 and 16 (both rainfed); b) Temporal evolution of the measured NDVI (circles) describing the crop growing cycle for fields 1, 13 and 16, along with the main phenology stages (BBCH scale) observed in the fields (41-45: Flag Leaf; 53-59: heading; 65: full flowering; 83-87: ripening); c) Temporal evolution of the water stress coefficient (K_{sw}), calculated through a soil water balance, in the fields 13 and 16.

4.2. Empirical values of harvest index and biomass production

The empirical data indicated a high variability of total biomass and HI values measured in the fields, see Table 5 and Table A 1. The average values and standard deviations (SD) of the total biomass and HI were 596 ± 101 g·m^{-2} and 0.37 ± 0.04 in rain-fed fields; 1299 ± 136 g·m^{-2} and 0.40 ± 0.02 in irrigated fields under water stress conditions; and 1847 ± 413 g·m^{-2} and 0.47

± 0.03 in irrigated fields under optimal water conditions. The average value of HI obtained in the whole dataset was 0.43 ± 0.06 reaching a maximum HI value of 0.55 and a minimum of 0.23, see Table A 1. The variability obtained for the measurement locations (Table A 1) was interpreted as the consequence of the inhomogeneity expected in commercial fields. These maximum and minimum values were considered as HI_x and HI_o respectively in order to calibrate the Equation 3.

According to the data analyzed in this study, the differences in total biomass production depend on the total water supply for the plants, quantified as irrigation plus precipitation during the growing season, see Table 5 and Figure 4a. In rain-fed fields the water supply, only precipitation, during the growing cycle was 171 ± 71 mm on average, the water supply for irrigated non-stressed fields was 603 ± 50 mm, and 343 ± 28 mm for irrigated but stressed fields (Fields 2 and 7). In contrast, the empirical values of HI depended on the percentage of water supply after anthesis, see Table 5 and Figure 4d. HI data is the result of the empirical determination of aboveground biomass and grain. Both measures are extremely variable in field conditions and the ratio between both is subjected to the obvious uncertainty and errors propagation. In consequence, the empirical data correlated in the Figure 4 presented dispersion around the least squares regression line.

As indicated in the Table 5, the rain-fed fields presented a remarkable dispersion in total water supply and water supply after anthesis and these differences resulted in strong differences in biomass and HI values. During 2018, the precipitation was, in general, higher and more frequent in the second half of the crop growing cycle than in 2017. In consequence, rain-fed crops reached greater total biomass and HI values in 2018.

Table 5. Average and standard deviation (SD) of total dry aboveground biomass ($g \cdot m^{-2}$), harvest index, total water supply (mm) and percentage of water supply after anthesis, according to the water management realized.

Water management	Biomass ($g \cdot m^{-2}$)	HI	Total water supply (mm)	% Water supply after anthesis over total water supply

Rainfed fields	596 ± 101	0.37 ± 0.04	171 ± 71	23 ± 21
Rainfed fields 2017	555 ± 121	0.36 ± 0.03	114 ± 34	6 ± 3
Rainfed fields 2018	637 ± 64	0.39 ± 0.04	229 ± 45	41 ± 15
Irrigated fields under water stress	1299 ± 136	0.40 ± 0.02	343 ± 28	26 ± 6
Irrigated fields without water stress	1847 ± 413	0.47 ± 0.03	603 ± 50	47 ± 10

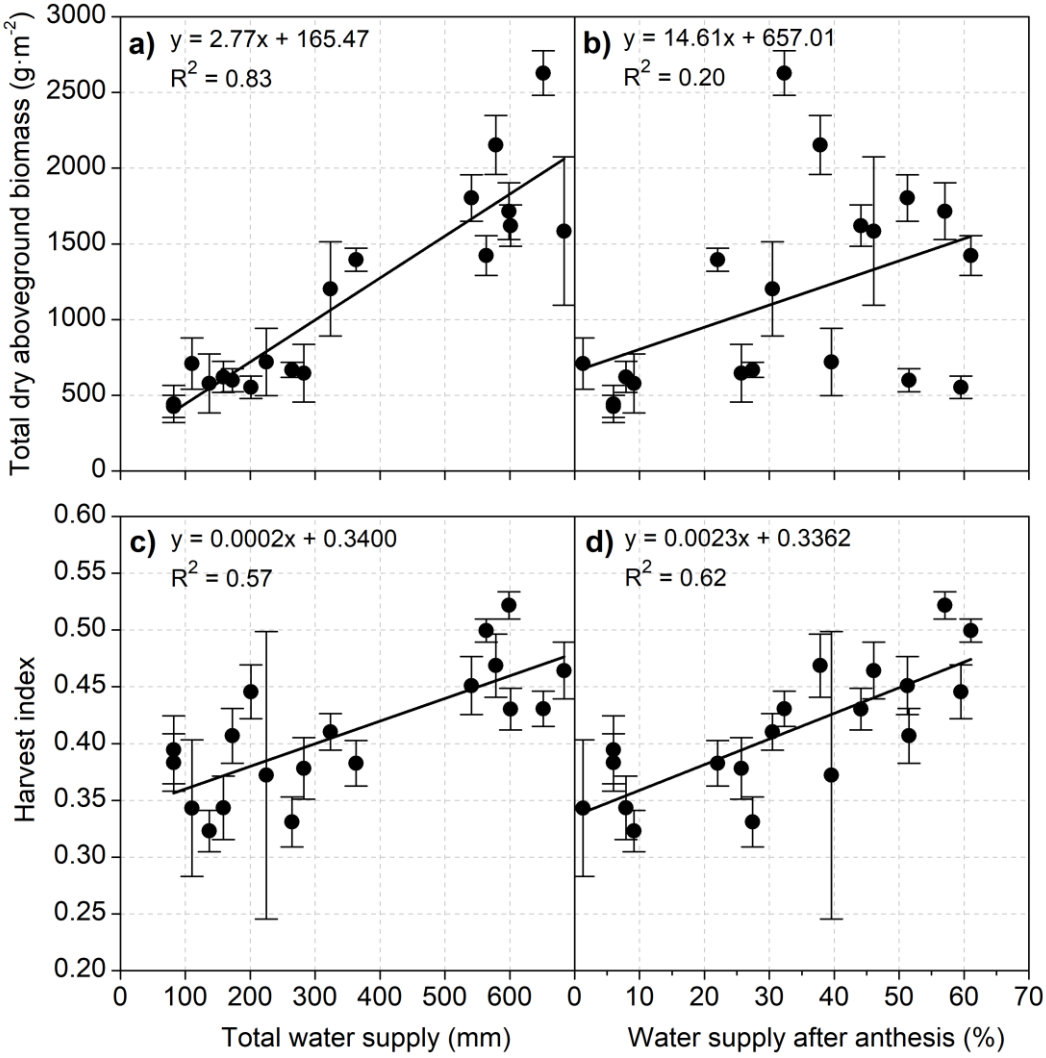

Figure 4. Correlation between average and standard deviation (SD) of total dry aboveground biomass ($g \cdot m^{-2}$) and harvest index (HI) measured in the study fields and total water supply (mm) and percentage or fraction of water supply after anthesis.

4.3. Estimation of the driving variables, θ_{APAR} , θ_T and $\theta_{Kt \cdot Kst}$

The estimated values of θ (θ_{APAR}, θ_T and $\theta_{Kt \cdot Kst}$) presented a high variability in the analyzed dataset. The minimum and maximum values obtained were around 0.1 and 0.5 (see Table 6 and Table 7), depending on the analyzed variable (θ_{APAR}, θ_T or $\theta_{Kt \cdot Kst}$). The average values of θ were

greater for the irrigated fields without water stress (Table 6) in agreement with the average values of HI measured in these fields (see Table 5). The average value varied depending on the variable used (APAR, T or $K_t \cdot K_{st}$) and were greater for the ratio based on transpiration (θ_T). The average values of θ and HI calculated for each field using the data obtained in each sampling zone (Table 7) were used to calibrate the proposed equations to estimate HI.

Table 6. Average and standard deviation (SD) of the estimated ratios according to the water management realized.

Water management	θ_{APAR}	θ_T	$\theta_{Kt \cdot Kst}$
Rainfed fields	0.15 ± 0.07	0.16 ± 0.07	0.15 ± 0.07
Irrigated fields under water stress	0.22 ± 0.01	0.25 ± 0.00	0.19 ± 0.02
Irrigated fields without water stress	0.41 ± 0.06	0.46 ± 0.05	0.36 ± 0.06

Table 7. Average and standard deviation (SD) of harvest index and estimated ratios in each study field.

Field	HI measured	θ_{APAR}	θ_T	$\theta_{Kt \cdot Kst}$
1	0.52 ± 0.01	0.48 ± 0.01	0.51 ± 0.01	0.43 ± 0.01
2	0.41 ± 0.02	0.23 ± 0.05	0.25 ± 0.05	0.21 ± 0.05
3	0.50 ± 0.01	0.51 ± 0.01	0.53 ± 0.01	0.47 ± 0.01
4	0.43 ± 0.02	0.38 ± 0.01	0.44 ± 0.01	0.32 ± 0.01
5	0.47 ± 0.03	0.37 ± 0.02	0.41 ± 0.02	0.31 ± 0.02
6	0.43 ± 0.02	0.35 ± 0.01	0.41 ± 0.01	0.30 ± 0.01
7	0.38 ± 0.02	0.22 ± 0.02	0.25 ± 0.02	0.18 ± 0.02
8	0.45 ± 0.03	0.38 ± 0.01	0.45 ± 0.02	0.35 ± 0.01
9	0.46 ± 0.02	0.38 ± 0.03	0.47 ± 0.04	0.35 ± 0.03
10	0.39 ± 0.03	0.14 ± 0.00	0.16 ± 0.00	0.12 ± 0.00
11	0.38 ± 0.03	0.16 ± 0.02	0.17 ± 0.02	0.14 ± 0.02
12	0.34 ± 0.03	0.08 ± 0.01	0.10 ± 0.01	0.08 ± 0.01
13	0.32 ± 0.02	0.09 ± 0.01	0.10 ± 0.01	0.08 ± 0.01
14	0.34 ± 0.06	0.11 ± 0.00	0.13 ± 0.00	0.10 ± 0.00
15	0.33 ± 0.02	0.11 ± 0.02	0.12 ± 0.02	0.12 ± 0.02
16	0.38 ± 0.03	0.08 ± 0.01	0.09 ± 0.01	0.09 ± 0.01
17	0.41 ± 0.02	0.27 ± 0.02	0.29 ± 0.02	0.27 ± 0.02
18	0.37 ± 0.13	0.25 ± 0.02	0.27 ± 0.02	0.24 ± 0.02
19	0.45 ± 0.02	0.19 ± 0.02	0.20 ± 0.03	0.21 ± 0.03

4.4. Calibration of HI relationships

The calibration parameters obtained from the linearization and used to calibrate the HI relationships proposed in this work, Equation 3 and Equation 4, are shown in the Table 8 and Table 9. The final relationships obtained are in Figure 5. Values of k obtained are within the range proposed by Kemanian *et al.*, (2007). However, the range of variability (SD) obtained in this study for each model were lower that the range obtained by those authors for a model based on

ground biomass measurements. We interpreted that this result indicated an increment on the precision for the estimation of harvest index. On the other hand, values of a and b obtained in this study are different from the calibration parameters presented by Sadras and Connor, (1991) and Richards and Townley-Smith, (1987) even considering the range of variability determined in our analysis.

Table 8. Calibration parameters of the Equation 3.

Ratio	**HI_x**	**HI_o**	**k**	**R^2**	**RMSE**
APAR			3.56 ± 0.20	0.75	0.031
Transpiration	0.55	0.23	3.18 ± 0.20	0.69	0.032
$K_t \cdot K_{st}$			3.93 ± 0.21	0.77	0.028

Table 9. Calibration parameters of the Equation 4.

Ratio	**a**	**b**	**R^2**	**RMSE**
APAR	0.079 ± 0.011	0.532 ± 0.018	0.76	0.027
Transpiration	0.079 ± 0.011	0.523 ± 0.017	0.74	0.028
$K_t \cdot K_{st}$	0.087 ± 0.011	0.550 ± 0.019	0.79	0.025

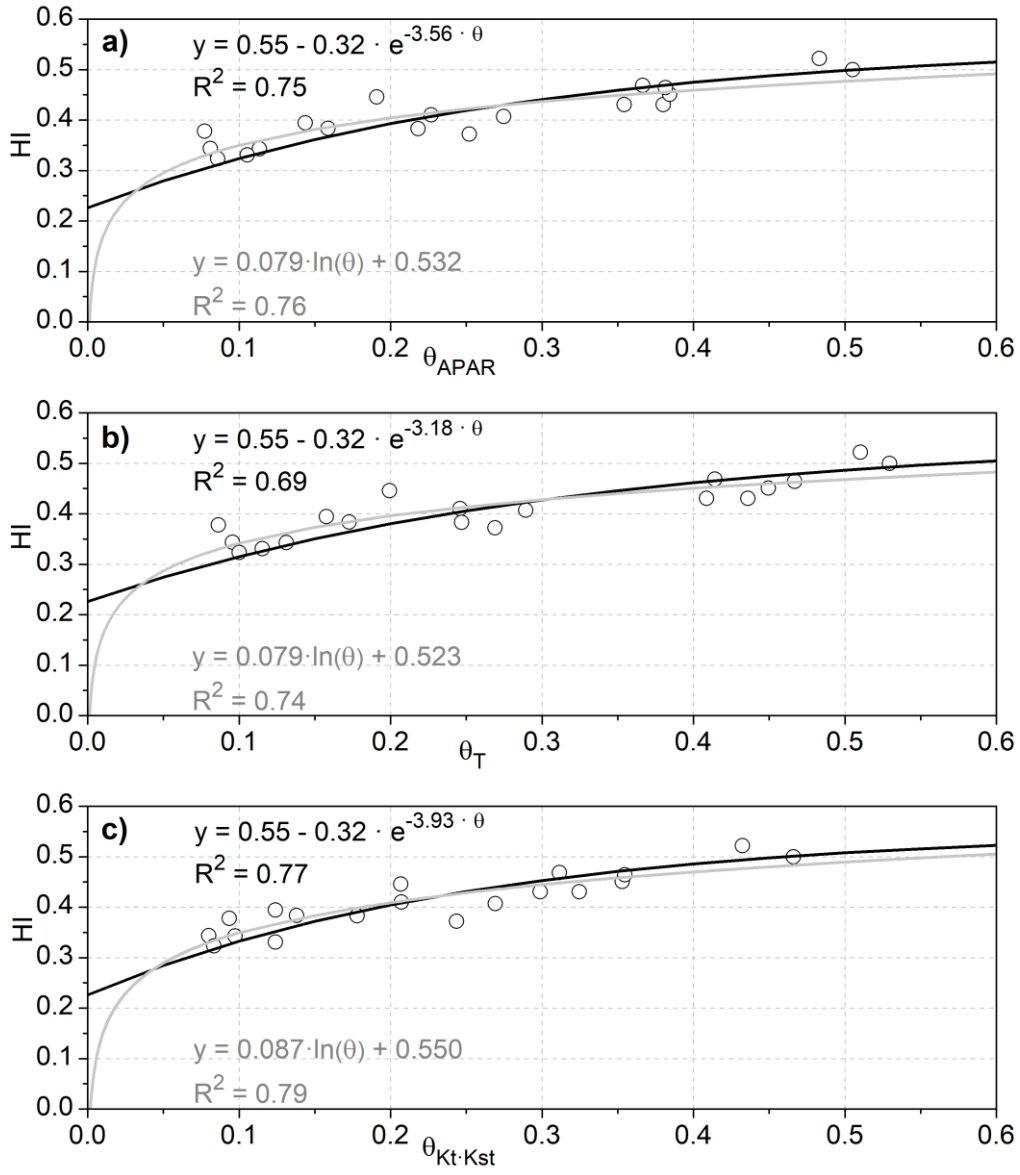

Figure 5. Correlation between the average values of harvest index measured and mean values estimated of a) ratio of photosynthetic active radiation absorbed by the vegetation (θ_{APAR}), b) ratio of crop transpiration (θ_T) and c) ratio of the product of the crop transpiration coefficient and the cold stress coefficient ($\theta_{Kt \cdot Kst}$) in each study field. Black lines show the calibration of exponential relationship (Equation 3) and grey lines represent the calibration of logarithmic relationship (Equation 4).

4.5. Analysis of the effect of water stress in the driving variables.

In the formulation proposed, the effect of water stress on HI is reflected through the variation of crop transpiration or radiation absorption and hence modifies the estimated values of θ. In addition, water stress determines the duration of the reproductive phase by causing accelerated senescence with respect to non-water stressed crops. This effect can be shown in

the time series NDVI images derived from the satellites, see Figure 3a. In consequence, we interpreted that the sole inclusion of the variables derived from NDVI, fPAR and K_t, in the models for the estimation of θ would reflect, at least in part, the effect of the water stress in the variables calculated and we analyzed if these ratios can reproduce, with similar exactitude, the variability of HI.

Table 10 shows the average values of θ calculated without including the daily values of water stress coefficient in the formulations proposed for the estimation of the biophysical parameters required (Equation 11, Equation 12 and Equation 13). These values are greater that the values of θ estimated considering the water stress conditions (Table 6) except for the irrigated fields without water stress. The reason for this difference is the presence of water stress mainly during post anthesis phase.

Table 10. Average and standard deviation (SD) of the estimated potential ratios, i.e. without including K_{sw}, in the estimation of required variables, according to the water management realized.

Water management	θ_{APAR} potential	θ_{T} potential	$\theta_{Kt \cdot Kst}$ potential
Rainfed fields	0.24 ± 0.08	0.26 ± 0.08	0.23 ± 0.07
Irrigated fields under water stress	0.28 ± 0.03	0.31 ± 0.02	0.25 ± 0.04
Irrigated fields without water stress	0.41 ± 0.06	0.46 ± 0.05	0.36 ± 0.06

Besides to the consideration of K_{sw} causes a drastic reduction of the estimated ratio compared to potential ratio in crops developed under sever water stress, see Figure 6, the average values of θ with and without considering the effect of water stress are linearly correlated for the crops monitored under water stress conditions. In our view, this correlation indicates that the potential development of specific relationships for the assessment of HI for crops under stress conditions by using proxy data like the effect of the stress on the canopy development (i.e. NDVI values) could be an interesting research line for future studies. However, the results obtained indicated the inter-annual variability of the noted relationship. In addition, the dataset analyzed in this study is scarce and the available data does not allow a more precise assessment of water stress conditions.

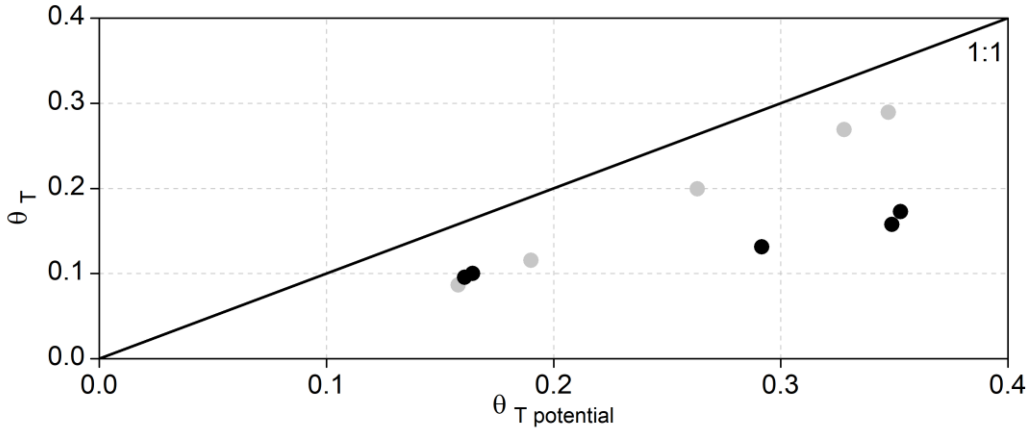

Figure 6. Relationship between transpiration ratio and potential transpiration ratio obtained for rainfed fields during campaign 2017 (black circles) and 2018 (grey circles).

5. DISCUSSION

5.1. Assessment of equations proposed for estimation of harvest index

The results obtained in the present study demonstrated the feasibility of remote sensing based approaches to estimate harvest index for wheat crop. The model proposed reproduced the inter-field variability of HI in a wide range of yields in commercial fields under different management conditions.

The use of different remote sensing-based biophysical variables related to crop physiology and meteorological data for estimation of the ratios is equivalent to the fraction of biomass or transpiration used by Kemanian *et al*.,(2007) and Sadras and Connor, (1991). Additional assumptions were a constant value of efficiencies (LUE, WUE, WP*) during the entire crop growing cycle and the consideration of no substantial variations of the biochemical composition of produced biomass during the post anthesis phase in wheat crops as proposed by (Sadras and Connor, 1991).

The analyses were realized with the average values of HI measured for each commercial field in order to reduce the effect of the high variability of HI values found within the fields. In addition, an independent dataset was not available to validate the calibrated equations but several tests were realized to analyze the robustness of the calibration parameters obtained. The calibration coefficients were similar, considering the range of variability quantified as SD, for subsets of the dataset or removing the data from several campaigns (2017, 2018) (not showed data). A later analysis was carried out considering HI values and estimated ratios calculated for each sampling zone (N = 96) and the analyses resulted in similar relationships that those showed in Figure 5 (not showed data).

Both proposed equations were able to reproduce of HI values measured in the fields with reasonable accuracy, although the logarithmic model achieved higher precision with higher R^2 and lower RMSE values. Moreover, each variable used for estimation of the ratio (APAR, T,

$K_t \cdot K_{st}$) provided a similar performance although the highest correlations were obtained for ratio based on $K_t \cdot K_{st}$, see Table 8 and Table 9.

5.2. Effect of water stress in the HI

According to empirical data, accumulated biomass and harvest index values vary depending on the water availability and irrigation management. These findings are consistent with the results obtained by de Wit, (1958) who reported that the biomass produced depends on the total amount water used, while HI depends on proportion of water used after anthesis. Our results indicated a strong linear relationship between the total amount of water used, this relationship has been analyzed for wheat in the same study area by Campos et al. (2018b), and the relationship between HI and the proportion of water used after anthesis is behind the models based on T and Kt analyzed in this paper.

The minimum value of HI (HI_o) obtained in this study was slightly lower than the range proposed by Kemanian *et al.*, (2007). The reason is the strong water shortage during post anthesis phase in rain-fed fields and resulted in HI values lower than 0.3 in some sub samples. In the same line, Richards and Townley-Smith, (1987) reported HI values below to 0.3 in dry enviroments, and Kobata *et al.*, (2018) also found lower HI values (below 0.1) in wheat species under rainfed conditions in the Mediterranen area. On the other hand, the maximum value of HI (HI_x) obtained in this work was within the range proposed in the curvilinear model for estimation of harvest index in wheat crops described by Kemanian *et al.*, (2007), and was higher than HI values reported it in the analyses of Sadras and Connor, (1991) and Richards and Townley-Smith, (1987). The reasons were presumably the progressive increase trend of HI values in modern wheat cultivars (Hay, 1995) which are used in the present work.

As mentioned previously, similar results were obtained for each calibrated equation proposed in this work and for the entire range of HI founded (0.23-0.55). However, the logarithmic equation could explain HI values close to zero reported by the literature in crops

under extreme water stress conditions. Nevertheless, further research is needed to analyze the effect of extreme water stress on harvest index.

Accelerated senescence in wheat crops is associated with reduced post-flowering plant water status (Fischer and Kohn, 1966), shortening the duration of the reproductive phase and decreasing the estimated ratios compared to non-stressed crops. The effects of water stress reducing the canopy growth and accelerating senescence is reflected in the time series of satellite multispectral imagery, while the effect of water stress on decreasing the actual transpiration is included in the methodology through the water stress coefficient (K_{sw}). The results indicated a severe water deficit (K_{sw}<1) in the analyzed rain-fed fields during the post flowering phase. These conditions caused a decrease in the transpiration rate and consequently, a drastic reduction on the estimated ratios and harvest index. According to the obtained results, and in agreement with existing knowledge, water used after anthesis is crucial to have high HI and therefore yield. This factual conclusion should be considered in the advice and design of crop calendars that prevent from limiting conditions/stresses during this period.

Effects of water stress are often confounded by nitrogen deficiency (Steduto *et al.*, 2012). As with effect of water stress, nitrogen stress causes a reduction on development of the canopy, which can be reflected by time series NDVI images. Effect of nitrogen stress on reducing rate biomass production (K_{sf}) can be expected similar to the effect of water stress (K_{sw}) but was not analyzed in this study. Previous studies (Campos *et al.*, (2018b) discussed that nitrogen deficits reducing the rate biomass production beyond to the obvious effects on canopy development are unusual under commercial fields managements as analyzed in this study.

As indicated before, the effects of water stress reducing the key variables was included in the methodology proposed by estimation of water stress coefficient (K_{sw}) using the water balance model described in FAO-56 manual. This model requires information about soil properties, e.g. field capacity, wilting point and soil depth, which could be available only in specific locations. However, the information required is not available for large areas and at field

scale, and therefore, the analyses performed assumed a typical soil in the study area for all analyzed fields. This assumption resulted in a plausible estimation of ratios and HI values in the analyzed rain-fed fields. Nevertheless, future works should analyze the variability of soil properties at field scale, spatializing the water stress coefficient and its effect on reducing the biomass production.

5.3. Assessment of the operational model

The results obtained in the present work promote the use of remote sensing as valuable tool for the operational estimation of harvest index in wheat crops at commercial field scale under a wide range of managements conditions using the calibrations parameters obtained in this study. The model presents clear advantages over the on-the-spot based approaches. The main operational advantage of the RS-based HI proposed approach is the capability to carry out HI estimates on commercial fields in large areas. The actual advantage of RS based biophysical parameters is that it reflects the actual conditions and in particular the effect of potential limitations to crop growth and expansion. Because of this advantage, already discussed and validated in previous research, the model is more operational and can be applied in great areas without the obvious limitations of data requirements. However, the two main limitations for operational applications are the assessment of crop water stress and the definition of the crop phenological stages as presented below.

In addition, this work enables further research on the estimation and spatial distribution of crop yield under different management conditions in commercial fields based on remote sensing data and considering HI variable values within the field. This interesting line of research is complementary to previous studies realized on estimation of accumulated biomass and within-field variability in wheat crops using a RS approach (Campos et al., 2018a,b). On the other hand, an additional source of uncertainty of the proposed operational model is that the effect of stresses is not considered. In this way, the proposed approach doesn´t consider possible

effects on reducing HI values, such as pollination failure due to cold or high temperature, pests, diseases or severe water deficit during the fruit setting, and probably actual HI values in these cases may be lower than the values estimated with this methodology.

The proposed approach uses soil water balance to estimate crop water stress. This stress impacts the actual values of HI reducing the biomass accumulation after anthesis. Water balance model requires a high number of variables (i.e. irrigation doses and amounts) and parameters (i.e. root depth), which are not widely available. Further methodologies that contribute to the assessment of crop water stress such as radar data or thermal remote sensing-based methods can be used and will result in a more operational approach. As many other approaches based on remote sensing, and specifically the use of multispectral vegetation indices, the proposed approach is limited in cloudy conditions. Moreover, the presence of weeds in the monitored fields could lead to overestimate biomass production and to affect the estimation of HI.

An additional weakness of the methodology proposed is the accurate determination of full flowering date (BBCH-65), being the key to calculate the noted ratios. As indicated in the section about methodology, the determination of full flowering date in was realized through observation and monitoring the crop phenology. However, this procedure is not feasible in an operational approach and at commercial field scale. Consequently, the authors propose the operational approach reported by González-Gómez *et al.*, (2018) who used different thermal times like growing-degree-days and accumulated reference evapotranspiration (ETo) among others and temporal evolution of NDVI to monitor phenology in wheat crops. According to these authors, full flowering phase requires about 300 mm of accumulated ETo and around 1050 GDD (growing degree days) from the green-up. However, water deficit can influence crop phenology, affecting the length of the development phases (McMaster *et al*., 2013), so the use of temporal scales to determine full flowering time in crops under water deficit could result in inaccurate results. Further research is needed to determine the consequences of water deficit in crop phenology and temporal scales.

6. CONCLUSIONS

This paper describes an operational methodology to estimate harvest index in commercial fields planted with wheat through its relationship with different ratios related to crop physiology. The proposed approach integrated time series of NDVI based on satellite remote sensing and meteorological data into the basis of the crop growth models for the estimation of the biophysical parameters.

The proposed equations for estimation of HI were calibrated for each variable used for the estimation of the required ratio (APAR, T, $K_t \cdot K_{st}$) using an extensive HI dataset obtained of 19 commercial fields in 4 campaigns under different water and nutrient managements.

The results obtained in this work demonstrated the ability of the methodology proposed to reproduce harvest index values under different management conditions and promote the use of Remote Sensing as an extraordinary tool to provide information about HI at field scale based on crop physiological parameters.

In addition, these results open the possibility for future research about the estimation of spatial distribution and within-field variability of crop yield under different management conditions.

ACKNOWLEDGEMENTS

This work was developed in the framework of projects HERMANA (HERramientas para el Manejo sostenible de Agua y Nutrientes en Agricultura) funded by the Spanish Ministry Science and Innovation (AGL2015-68700-R) and FATIMA (FArming Tools for external nutrient Inputs and water MAnagement), funded by the European Union´s Horizon 2020 research and innovation programme (Grant Agreement No 633945). The authors would like to recognize the effort of the people who actively involved in data collection and sample processing (J. Villodre, L. González, S. Sánchez and A. Rodríguez from IDR-UCLM, N. Jimenez from AgriSat Iberia S.L. and E. Pareja, F.M. Jara and P. Avilés from Instituto Técnico Agronómico Provincial).

References

Allen, R.G., Raes, D., Smith, M., 1998. Crop Evapotranspiration: Guidelines for Computing Crop Requirements, Irrig. Drain. Pap. No. 56, FAO, Rome, Italy.

Asrar, G., Fuchs, M., Kanemasu, E.T., Hatfield, J.L., 1984. Estimating Absorbed Photosynthetic Radiation and Leaf Area Index from Spectral Reflectance in Wheat. Agron. J. 76, 300–306.

Beaven, E.S., 1920. Breeding Cereals for Increased Production. Journ. Farmers' Club Part VI.

Brown, H.E., Moot, D.J., Teixeira, E.I., 2006. Radiation use efficiency and biomass partitioning of lucerne (Medicago sativa) in a temperate climate. Eur. J. Agron. 25, 319–327.

Calderini, D.F., Abeledo, L.G., Slafer, G.A., 2000. Physiological maturity in wheat based on kernel water and dry matter. Agron. J. 92, 895–901.

Calera, A., Campos, I., Osann, A., D'Urso, G., Menenti, M., 2017. Remote sensing for crop water management: From ET modelling to services for the end users. Sensors 17, 1–25.

Campos, I., Balbontín, C., González-Piqueras, J., González-Dugo, M.P., Neale, C.M.U., Calera, A., 2016. Combining a water balance model with evapotranspiration measurements to estimate total available soil water in irrigated and rainfed vineyards. Agric. Water Manag. 165, 141–152.

Campos, I., González-Gómez, L., Villodre, J., Calera, M., Campoy, J., Jiménez, N., Plaza, C., Sánchez-Prieto, S., Calera, A., 2018a. Mapping within-field variability in wheat yield and biomass using remote sensing vegetation indices. Precis. Agric.

Campos, I., González-Gómez, L., Villodre, J., González-Piqueras, J., Suyker, A.E., Calera, A., 2018b. Remote sensing based crop biomass with water or light-driven crop growth models in wheat commercial fields. F. Crop. Res. 216, 175–188.

Campos, I., Neale, C.M.U., Suyker, A.E., Arkebauer, T.J., Gonçalves, I.Z., 2017. Reflectance-based crop coefficients REDUX: For operational evapotranspiration estimates in the age of high producing hybrid varieties. Agric. Water Manag. 187, 140–153.

Campoy, J., Campos, I., Plaza, C., Calera, M., Jiménez, N., Bodas, V., Calera, A., 2019. Water use efficiency and light use efficiency in garlic using a remote sensing- based approach. Agric. Water Manag. 219, 40–48.

Chen, X., Vierling, L., Deering, D., 2005. A simple and effective radiometric correction method to improve landscape change detection across sensors and across time. Remote Sens. Environ. 98, 63–79.

Choudhury, B.J., Ahmed, N.U., Idso, S.B., Reginato, R.J., Daughtry, C.S.T., 1994. Relations between evaporation coefficients and vegetation indices studied by model simulations. Remote Sens. Environ. 50, 1–17.

Daughtry, C.S.T., Gallo, K.P., Goward, S.N., Prince, S.D., Kustas, W.P., 1992. Spectral estimates of absorbed radiation and phytomass production in corn and soybean canopies. Remote Sens. Environ. 39, 141–152.

de Wit, C.T., 1958. Transpiration and crop yields. Versl. Landbouwk. Onderz. 64. 6. 88.

Dodds, M.E., Bowren, K.E., Dew, D.A., Faris, D.G., 1979. The effect of windrowing hard red spring wheat at different stages of maturity at four locations in Western Canada. Can. J. Plant Sci 59, 321–328.

Donald, C.M., 1962. In search of yield. J. Aust. Inst. Agric. Sci 238, 171–178.

Donald, C.M., Hamblin, J., 1976. The Biological Yield and Harvest Index of Cereals as Agronomic and Plant Breeding Criteria. Adv. Agron. 28, 361–405.

Duchemin, B., Hadria, R., Erraki, S., Boulet, G., Maisongrande, P., Chehbouni, A., Escadafal, R., Ezzahar, J., Hoedjes, J.C.B., Kharrou, M.H., Khabba, S., Mougenot, B., Olioso, A., Rodriguez, J.C., Simonneaux, V., 2006. Monitoring wheat phenology and irrigation in Central Morocco: On the use of relationships between evapotranspiration, crops coefficients, leaf area index and remotely-sensed vegetation indices. Agric. Water Manag. 79, 1–27.

Fischer, R.A., Kohn, G.D., 1966. The relationship of grain yield to vegetative growth and post-flowering leaf area in the wheat crop under conditions of limited soil moisture. Aust. J. Agric. Res. 17, 281–295.

González-Dugo, M.P., Mateos, L., 2008. Spectral vegetation indices for benchmarking water productivity of irrigated cotton and sugarbeet crops. Agric. Water Manag. 95, 48–58.

Gonzalez-Dugo, M.P., Neale, C.M.U., Mateos, L., Kustas, W.P., Prueger, J.H., Anderson, M.C., Li, F., 2009. A comparison of operational remote sensing-based models for estimating crop evapotranspiration. Agric. For. Meteorol. 149, 1843–1853.

González-Gómez, L., Campos, I., Calera, A., 2018. Use of different temporal scales to monitor phenology and its relationship with temporal evolution of normalized difference vegetation index in wheat. J. Appl. Remote Sens. 12, 1–18.

Hay, R.K.M., 1995. Harvest index: A review of its use in plant breeding and crop physiology. Ann. Appl. Biol. 126, 197–216.

Hsiao, T.C., 1973. Plant Responses to water stress. Annu. Rev. Plant Physiol. 24, 519–570.

Kemanian, A.R., Stöckle, C.O., Huggins, D.R., Viega, L.M., 2007. A simple method to estimate harvest index in grain crops. F. Crop. Res. 103, 208–216.

Kobata, T., Koç, M., Barutçular, C., Tanno, K. ichi, Inagaki, M., 2018. Harvest index is a critical factor influencing the grain yield of diverse wheat species under rain-fed conditions in the Mediterranean zone of southeastern Turkey and northern Syria. Plant Prod. Sci. 21, 71–82.

Lobell, D.B., Ortiz-Monasterio, J.I., Sibley, A.M., Sohu, V.S., 2013. Satellite detection of earlier wheat sowing in India and implications for yield trends. Agric. Syst. 115, 137–143.

McMaster, G.S., Ascough, J.C., Edmunds, D.A., Nielsen, D.C., Prasad, P.V.V., 2013. Simulating crop phenological responses to water stress using the PhenologyMMS software program. Appl. Eng. Agric. 29, 233–249.

Padilla, F.L.M., González-Dugo, M.P., Gavilán, P., Domínguez, J., 2011. Integration of vegetation indices into a water balance model to estimate evapotranspiration of wheat and corn. Hydrol. Earth Syst. Sci. 15, 1213–1225.

Passioura, J.B., 1977. Grain yield, harvest index and water use of wheat. J. Aust. Institure Agric. Sci. 43, 117–120.

Raes, D., Steduto, P., Hsiao, T.C., Fereres, E., 2011. AquaCrop Reference Manual, FAO–Land and water Division. FAO, Land and Water Division, Rome, Italy.

Richards, R.A., Townley-Smith, T.F., 1987. Variation in leaf area development and its effect on water use, yield and harvest index of droughted wheat. Aust. J. Agric. Res. 38, 983–992.

Ritchie, J.T., 1998. Soil water balance and plant water stress, in: Tsuji, G.Y., Hoogenboom, G., P.K., T. (Eds.), Understanding Options for Agricultural Production. Systems Approaches for Sustainable Agricultural Development,Vol 7. Springer, Dordrecht, pp. 41–54.

Sadras, V.O., Connor, D.J., 1991. Physiological basis of the response of harvest index to the fraction of water transpired after anthesis: A simple model to estimate harvest index for determinate species. F. Crop. Res. 26, 227–239.

Sellers, P.J., Los, S.O., Tucker, C.J., Justice, C.O., Dazlich, D.A., Collatz, G.J., Randall, D.A., 1996. A revised land surface parameterization (SiB2) for atmospheric GCMs. Part II: The generation of global fields of terrestrial biophysical parameters from satellite data. J. Clim.

Steduto, P., Hsiao, T.C., Fereres, E., Raes, D., 2012. Crop yield response to water, Fao Irrigation and Drainage Paper Issn.

Stöckle, C.O., Donatelli, M., Nelson, R., 2003. CropSyst, a cropping systems simulation model. Eur. J. Agron. 18, 289–307.

Szeicz, G., 1974. Solar radiation for plant growth. J. Appl. Ecol. 11, 617–636.

Williams, J.R., Jones, C.A., Kiniry, J.R., Spanel, D.A., 1989. The EPIC Crop Growth Model. Trans. ASAE 32, 0497–0511.

ANNEX I. EMPIRICAL DATA OBTAINED IN THE SUB-SAMPLES IN THE STUDY FIELDS.

Table A 1. Dry aboveground biomass (B, g·m^{-2}), dry grain yield (Y, g·m^{-2}) and harvest index (HI, dimensionless) measured in each sub sample realized in the study fields.

ID/ Points		1A	1B	1C	2A	2B	2C	3A	3B	3C	4A	4B	4C	5A	5B	5C	6A	6B	6C	7A	7B	7C	8A	8B	8C	9A	9B	9C	10A	10B	10C	11A	11B	11C	12A	12B	12C
1	B	1806	1824	1895	1922	1517	1634	2057	1742	1722		1594	1699	1294	1489	1530	1695	1586	1533	1887	1789	1804	2065	2010			1436	1596										
	Y	954	949	996	1008	796	904	1074	862	846		798	906	716	785	795	883	833	791	979	931	938	1080	984			784	839										
	HI	0.53	0.52	0.53	0.52	0.53	0.55	0.52	0.49	0.49		0.50	0.53	0.55	0.53	0.52	0.52	0.53	0.52	0.52	0.52	0.52	0.52	0.49			0.55	0.53										
2	B	939	1155		1067	1062	1036	1641	1600	1633	734	926	965		778	940	1547		1327	1259			1732		1623	992												
	Y	359	470		439	449	388	675	680	699	322	368	455		322	377	625		581	481			736		633	416												
	HI	0.38	0.41		0.41	0.42	0.37	0.41	0.42	0.43	0.44	0.40	0.47		0.41	0.40	0.40		0.44	0.38			0.43		0.39	0.42												
3	B			1637	1832	1588	1459	1408	1325	1290	1282		1580	1242	1517	1135	1210	1462	1524	1308	1437	1612	1273	1294		1424	1150	1448										
	Y			820	878	814	732	735	674	645	578		809	617	730	558	619	698	755	659	736	806	658	662		696	597	715										
	HI			0.50	0.48	0.51	0.50	0.52	0.51	0.50	0.45		0.51	0.50	0.48	0.49	0.51	0.48	0.50	0.50	0.51	0.50	0.52	0.51		0.49	0.52	0.49										
4	B	1566	1593	1757	1399	1424	1729	1527	1688	1768	1948	1663	1839	1508	1749	1756	1725	1195	1338																		
	Y	681	611	795	596	651	666	714	730	829	734	672	784	766	703	700	654	549	646																		
	HI	0.43	0.38	0.45	0.43	0.46	0.39	0.47	0.43	0.47	0.38	0.40	0.43	0.51	0.40	0.40	0.38	0.46	0.48																		
5	B	2407	1800	1726	1959	1846	2066	2758	2575	2108	1966	2374	2164	2406	2250	2080	2078	1978	2219																		
	Y	995	840	774	940	867	981	1159	1115	907	979	1102	1007	1220	1088	1015	1050	965	1111																		
	HI	0.41	0.47	0.45	0.48	0.47	0.47	0.42	0.43	0.43	0.50	0.46	0.47	0.51	0.48	0.49	0.51	0.49	0.50																		
6	B	2404	2741	2601	2655	2419	2703	3134	2521	1888	2161	2576	2651	2870	3191	2391	2474	3486	2438																		
	Y	1103	1199	1091	1213	1120	1192	1229	1108	813	900	1094	1188	1209	1415	1036	889	1319	1188																		
	HI	0.46	0.44	0.42	0.46	0.46	0.44	0.39	0.44	0.43	0.42	0.42	0.45	0.42	0.44	0.43	0.36	0.38	0.49																		
7	B	1402	1310	1500	1316	1599	1447	1187	1167	1466	1336	1512	1428	1327	1405	1278	1568	1373	1485																		
	Y	520	527	529	485	601	506	464	427	594	484	585	492	481	531	534	659	594	596																		
	HI	0.37	0.40	0.35	0.37	0.38	0.35	0.39	0.37	0.41	0.36	0.39	0.34	0.36	0.38	0.42	0.42	0.43	0.40																		
8	B	1658	1524	1750	1577	1915	1950	2033	2086	1734																											
	Y	722	671	794	731	946	938	814	949	756																											
	HI	0.44	0.44	0.45	0.46	0.49	0.48	0.40	0.46	0.44																											
9	B	942	1113	1000	1728	1952	1863	1823	1899	1934																											
	Y	426	569	514	837	897	794	817	817	880																											
	HI	0.45	0.51	0.51	0.48	0.46	0.43	0.45	0.43	0.46																											
10	B	214	354	361	583	629	446	558	495	339																											
	Y	73	135	133	239	242	173	233	196	155																											
	HI	0.34	0.38	0.37	0.41	0.38	0.39	0.42	0.40	0.46																											
11	B	364	342	339	372	434	675	428	520	361																											
	Y	143	125	122	125	169	248	198	194	144																											
	HI	0.39	0.37	0.36	0.34	0.39	0.37	0.46	0.37	0.40																											
12	B	516	568	427	711	705	577	633	643	808																											
	Y	202	216	151	267	224	180	183	205	287																											
	HI	0.39	0.38	0.35	0.38	0.32	0.31	0.29	0.32	0.35																											
13	B	392	410	386	573	566	527	727	827	794																											
	Y	128	125	106	187	211	156	259	268	258																											
	HI	0.33	0.30	0.28	0.33	0.37	0.30	0.36	0.32	0.33																											
14	B	647	587	557	575	647	661		871	935																											
	Y	214	139	159	171	223	251		327	406																											
	HI	0.33	0.24	0.29	0.30	0.34	0.38		0.38	0.43																											
15	B	545	841	715	655	579	595	749	739	592																											
	Y	197	275	255	196	221	199	233	200	200																											
	HI	0.36	0.33	0.36	0.30	0.38	0.33	0.31	0.27	0.34																											
16	B	539		390	875	746	910	590	641	651																											
	Y	216		140	345	306	371	215	201	243																											
	HI	0.40		0.36	0.39	0.41	0.41	0.36	0.31	0.37																											
17	B	469	473	596	622	742	532	558	763	641																											
	Y	200	197	271	217	288	221	212	326	260																											
	HI	0.43	0.42	0.45	0.35	0.39	0.42	0.38	0.43	0.41																											
18	B	477			947	674	690	883	976	882																											
	Y	108			409	303	324	388	425	392																											
	HI	0.23			0.43	0.45	0.47	0.44	0.44	0.44																											
19	B	543	488	515	478	566	516	711	690	645	422	557	484	553	612	520	554	403	694	507	448	639	552	455	521	578	536	645	274	565	553	473	452	594	641	749	726
	Y	243	207	231	204	248	216	334	324	290	199	241	204	226	266	213	241	165	323	222	201	279	230	187	228	239	224	292	113	278	265	242	230	290	304	362	315
	HI	0.45	0.42	0.45	0.43	0.44	0.42	0.47	0.47	0.45	0.47	0.43	0.42	0.41	0.43	0.41	0.44	0.41	0.47	0.44	0.45	0.44	0.42	0.41	0.44	0.41	0.42	0.45	0.41	0.49	0.48	0.51	0.51	0.49	0.47	0.48	0.43